applied sciences

MDPI

Article

Study on the Effect of Micro-Vessels on Ablation Effect in Laser Interstitial Brain Tissue Thermal Therapy Based on PID Temperature Control

Sixin Bi [1,2], Huihui Liu [1,2], Qun Nan [1,2,*] and Xin Mai [1,2]

[1] Faculty of Environment and Life, Beijing University of Technology, Beijing 100124, China; bsx_ymwym@163.com (S.B.); liuhuihui19990102@163.com (H.L.); mxmaixin@163.com (X.M.)
[2] Beijing International Science and Technology Cooperation Base for Intelligent Physiological Measurement and Clinical Transformation, Beijing 100124, China
* Correspondence: nanqun@bjut.edu.cn

Abstract: Laser interstitial thermal therapy (LITT) is an emerging clinical treatment for deep brain tumors, which is safe, minimally invasive, and effective. This paper established a three-dimensional model based on the LITT heat transfer model, including brain tissue, laser fiber, and straight tube vessels. Combining the PID control equation, diffuse approximation equation, Pennes heat transfer equation, and Murray's law, the effect of micro-vessel radius and distance between vessels and fiber on the ablation temperature field during laser ablation was investigated by using COMSOL finite element software. The results showed that at a constant distance of 1 mm between the vessel and the fiber, the vessels with a radius of 0.1–0.2 mm could be completely coagulated, the vessels with a radius of 0.3–0.6 mm had cooling and directional effects on temperature distribution and thermal damage, and the vessels with a radius of 0.7–1.0 mm had cooling effects on the ablation temperature. When the vessel-fiber spacing was raised by 2 mm, 0.3–0.4 mm, vasculature had a directional influence on the temperature field; when the vessel-fiber spacing was raised by 3 mm, only 0.3 mm vessels had a directional effect on the temperature field. The range of temperature field impacted by blood flow diminishes as the distance between the optical fiber and the blood artery grows. The ablation zone eventually tends to be left and right symmetrical. In this study, we simulated the LITT ablation temperature field model influenced by tiny vessels based on PID control. We initially classified the vessels, which provided some guidance for accurate prediction and helped the accuracy of preoperative planning.

Keywords: laser interstitial thermal therapy; PID temperature control; temperature distribution; directional effect

check for updates

Citation: Bi, S.; Liu, H.; Nan, Q.; Mai, X. Study on the Effect of Micro-Vessels on Ablation Effect in Laser Interstitial Brain Tissue Thermal Therapy Based on PID Temperature Control. *Appl. Sci.* **2023**, *13*, 3751. https://doi.org/10.3390/app13063751

Academic Editor: Piotr Gas

Received: 15 February 2023
Revised: 13 March 2023
Accepted: 13 March 2023
Published: 15 March 2023

Copyright: © 2023 by the authors. Licensee MDPI, Basel, Switzerland. This article is an open access article distributed under the terms and conditions of the Creative Commons Attribution (CC BY) license (https://creativecommons.org/licenses/by/4.0/).

1. Introduction

Brain tumors are one of the health problems that cause worldwide concern. Their incidence is increasing year by year and can occur at any age, accounting for 5% of adult tumor incidence and 70% of childhood tumor incidence [1], and they account for 1.4% of all cancers and 2.4% of all cancer deaths [2]. Common treatment methods include surgery, radiotherapy, and chemotherapy, but at present, the above methods have limitations for patients with brain tumors that are located deeper, adjacent to functional brain areas, difficult to reach by surgical route, and in poor general condition, so thermal ablation has become one of the scientifically effective methods. The treatment principle of this procedure is to cause coagulation necrosis of brain tumor cells through local high temperatures with minimal damage to the surrounding normal brain tissue.

Laser Interstitial Thermal Therapy (LITT) technique is safe, minimally invasive, and effective for lesions that are more difficult to access through open access, deeper lesions, and patients who may not be able to tolerate open surgery. Therefore, it has become the

most commonly used ablation technique for the treatment of brain tumors worldwide. LITT uses light to produce a photothermal effect in the tissue to cause coagulation necrosis of brain tumor cells [3]. The clinical application is guided by magnetic resonance imaging. One or more optical fibers are delivered to the patient's brain tumor, where the laser is deposited at low power and a long exposure time, increasing the temperature in the target area for tissue destruction [4]. When ablating under-exposed intracranial tumors, the target temperature of LITT is set at 45–90 °C [5], which achieves the critical temperature for tissue necrosis to occur while avoiding charring and vaporization of the tissue due to high temperature. At the same time, edema is also avoided because the transition zone between the target area and the surrounding normal brain tissue is less than 1 mm. To accurately predict the temperature change and damage in the focal area, more and more scholars have proposed exploring the temperature field changes by real-time simulation and reconstruction of the tumor/surrounding tissue in the target area through finite element simulation techniques [6,7].

However, various related studies have shown that tumor tissue usually grows more abundantly near blood vessels. During laser heating, the blood flow in the blood vessels takes away some of the heat and affects the distribution of the temperature field. The micro-vessels system in the tissue is disrupted during ablation, and the blood vessels near the target area are prone to coagulation effects. At the same time, the imaging techniques currently used in clinical practice (e.g., conventional CT and MRI) have too low a resolution in detecting small vessels [8] (<1 mm in diameter), making the study of small vessel effects necessary. Sheu et al. [9] presented an energy equation for tissue heating and split the regions of interest into tissue perfusion areas and blood vessel-containing capillary areas. Andreozzi et al. [10] considered the effect of four different vessels on the ablation situation in capillaries, terminal arteries, terminal branches of arteries, and tertiary branches to make the simulation more realistic. Still, they focused on using each vessel as a liquid phase to explore the effect of porous media on the temperature field. To assess the small vessel heat transfer mechanism during the heating of biological tissues, Hassanpour and Saboonchi [11] suggested a study approach to model cylindrical parallel tiny vessels as forward/reverse flow vascular networks. The approximate modeling of blood vessels was performed using the Pennes equation and the one-dimensional convective diffusion equation (constant heat transfer coefficient of the blood vessel wall). They discovered that when distance shrank, blood vessel volume grew, there were more blood vessel branches, and the cooling impact grew. Huang [12] explored the effect of a single vessel and a pair of parallel convective vessels with 1 mm and 2 mm diameters, respectively, on the blood flow characteristics in the coagulation zone. It was found that the thermal damage caused by RF electrodes perpendicular to the vessel was smaller in volume than that caused by parallel vessels and that the low flow rate in large vessels resulted in "tail-like" thermal lesions that damaged the tissue downstream of the vessel. Nikhil [13] studied the dependence of the heat transfer coefficient of the small vessel wall on geometric parameters and found that the vessel has a directional influence on the temperature field, but only the variation of the temperature field at a fixed distance was considered.

The purpose of this work is to investigate the influence of small blood veins on the laser Interstitial Thermal Therapy temperature field. We have developed a model of parallel straight tubular micro-vessels (less than 1 mm radius) and brain tissue, considering dynamic photothermal effects, where the blood flow velocity is dynamically varied by vessel diameter. The cooling and directional effects of blood vessel diameter and distance between the blood vessel and optical fiber on temperature distribution were analyzed. In addition, some experience has been gained in the application of computer simulations and can therefore be applied to assist in the preoperative planning of clinical LITT.

2. Materials and Methods

In this section, based on the finite element method, the finite element simulation software COMSOL Multiphysics 5.5 (COMSOL Inc., Palo Alto, CA, USA) was applied to

model the brain tissue for LITT. Combined with PID governing equation, the laser incident power is obtained, and the radial and axial laser energy is obtained by substituting the Gaussian distribution equation. The diffusion approximate equation is used to simulate the optical field distribution. The irradiance is used as the heat source term of Pennes heat transfer equation to simulate the temperature field. Murray's law was used to calculate vascular flow, and the Arrhenius equation was used to calculate thermal damage. Dynamic photo-thermal parameters are also used. The interaction between tiny blood vessels and the temperature field during laser ablation was analyzed. Related geometric models and equations are described in the following sections.

2.1. Model Geometry

The computational geometry, as in Figure 1, includes an ideal rectangular brain tissue region with a length*width*height of 20 mm and assumed to be isotropic and homogeneous; a simplified laser fiber with a radius of 0.4 mm and a length of 12.5 mm, a target head length of 5 mm, with a thin 0.1 mm shell and a water-cooled structure; and a straight tube vessel of variable diameter, ignoring fine perfusion.

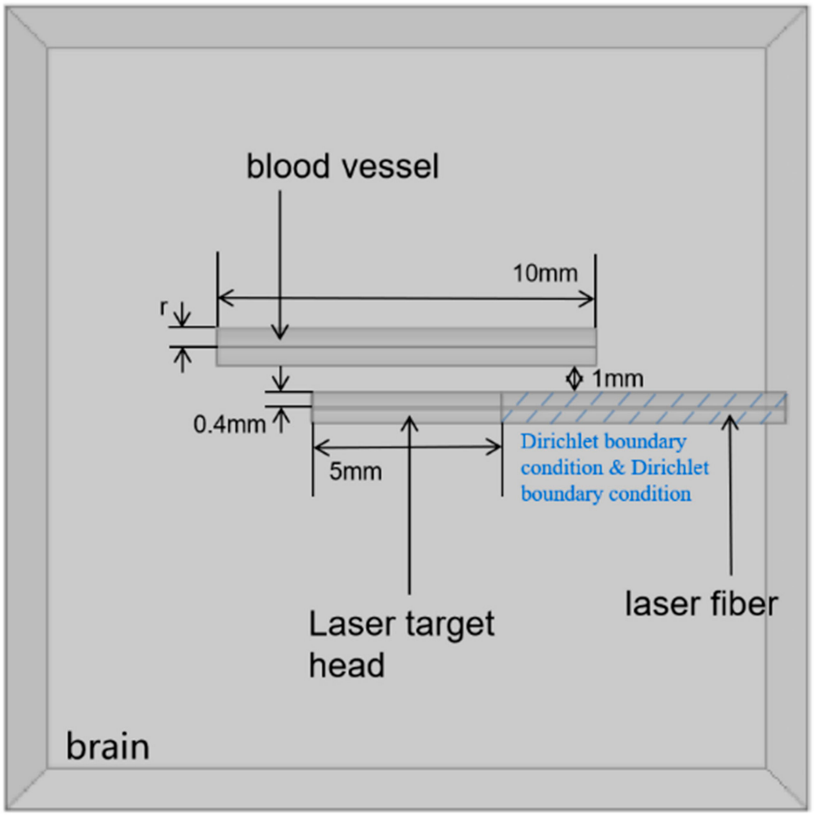


Figure 1. Model geometry.

2.2. Mathematical Models

The PID control algorithm contains proportional control, integral control, and differential control of deviation. It works as shown in Figure 2, which can achieve intelligent control of laser power automatic adjustment by adjusting parameters. To control the temperature in the center of the fiber targeting area, which relies solely on the working experience of the medical personnel and lacks a precise temperature control mechanism, the PID control algorithm is introduced to control the maximum fiber temperature at 90 °C. The specific control equation is shown in Equations (1) and (2) [14]:

$$P_{in} = K_p \cdot e(t) + K_i \cdot \int_o^t e(t)dt + K_d \cdot \frac{d[e(t)]}{dt} \quad (1)$$

$$e(t) = T_{\text{set}} - T_{\text{tip}} = 90\ ^{\circ}\text{C} - T_{\text{tip}} \quad (2)$$

where P_{in} is the feedback power (W) under PID control, K_p is the proportional control coefficient, K_i is the integral control coefficient, K_d is the differential control coefficient, $e(t)$ is the temperature deviation (°C) at the time t(s), T_{set} is the set target temperature (90 °C), and T_{tip} is the actual measured temperature (°C).

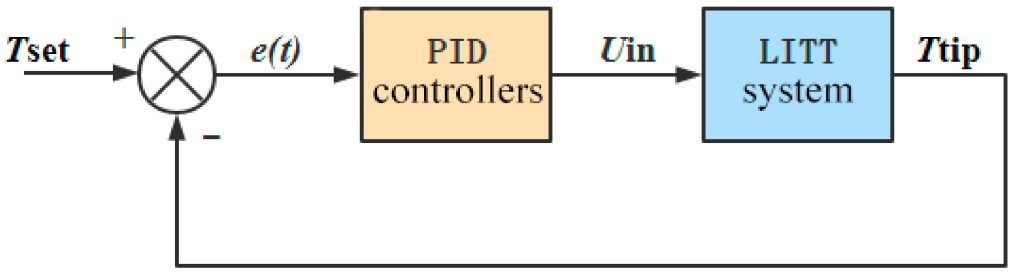


Figure 2. PID control principle.

After adjustment, the temperature diagram of the domain point probe and the temperature distribution diagram of LITT is shown in Figures 3 and 4.

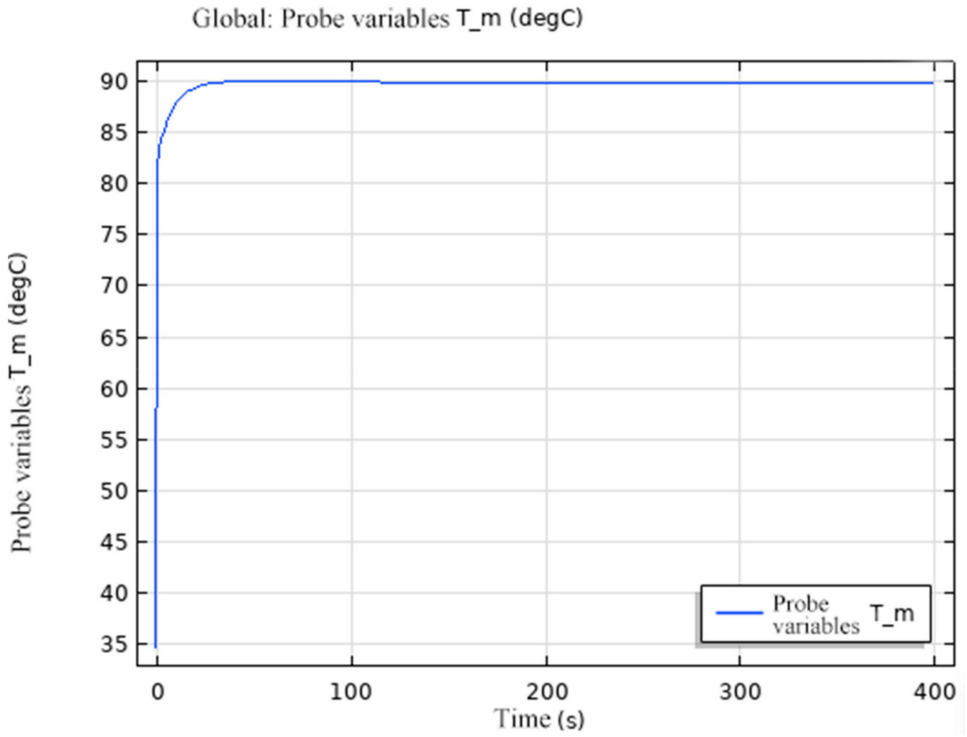


Figure 3. Temperature diagram of domain point probe after adjustment.

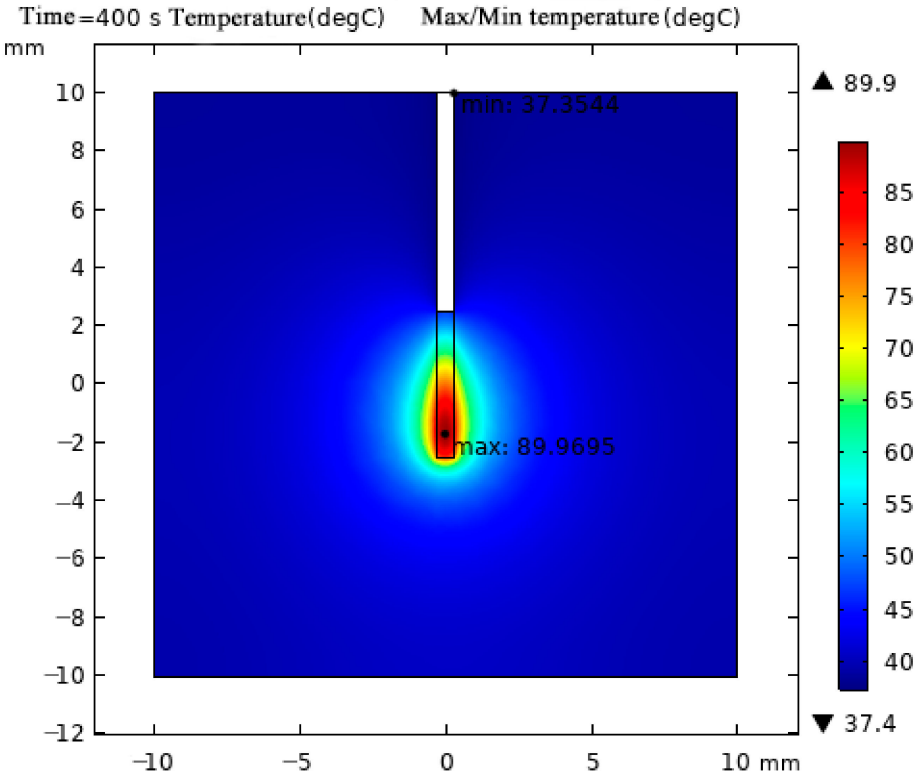


Figure 4. PID control LITT temperature distribution chart.

In the LITT simulation process, light enters the tissue due to scattering to form the angle of diffuse light approximation into an isotropic state, and the laser irradiance is calculated by applying the diffuse approximation equation as shown in Equations (3) and (4) [15,16]. The light propagates in the fiber and diffuses outward after reaching the target head, mainly divided into radial and axial diffusion in spatial distribution. For simplicity, the current model assumes that the laser intensity consists of two directional laser powers: the radial direction of the diffusion part, P1 (assuming 95% of the incident laser power, with the incident power being the feedback power Pin under PID control), in a fiber super-Gaussian distribution [15]; and the axial direction, P2 (assuming 5% of the incident laser power), in a Gaussian distribution [17], as shown in Equations (5) and (6).

Laser irradiance

$$\mu_a \Phi(x,y,z) - D\nabla^2 \Phi(x,y,z) = s(x,y,z) \tag{3}$$

$$D = \frac{1}{3(\mu_a + \mu_s(1-g))},\ s(x,y,z) = \mu_s(1-g)(QJ + QZ) \tag{4}$$

Radial super-Gaussian distribution equation

$$QJ = k \cdot \frac{P1}{2\pi w l} \cdot e^{-2(\frac{z}{\sigma})^p} \cdot e^{-(\mu_a+\mu_s(1-g))\sqrt{x^2+y^2}} \tag{5}$$

Axial Gaussian distribution equation

$$QZ = \frac{P2}{2\pi\sigma^2} \cdot e^{\frac{-(x^2+y^2)}{2\sigma^2}} \cdot e^{-(\mu_a+\mu_s(1-g))z} \tag{6}$$

where $\Phi(x, y, z)$ is the laser irradiance (W/m^2), QJ is the laser irradiance in the radial direction (W/m^2), and QZ is the laser irradiance in the axial direction (W/m^2); μ_a is the absorption coefficient (1/m), μ_s is the scattering coefficient (1/m), g is the anisotropic factor, D is the diffusion constant in the tissue (m), w is the fiber radius (mm), l is the fiber length

(mm), σ is the Gaussian distribution deviation [18], p is the super-Gaussian distribution order [18], and k is the loss factor [19].

The deposition of light in the tissue produces a photothermal effect, and the Pennes heat transfer equation is used to study the heat transfer in the tissue, as shown in Equation (7) [20]:

$$\rho c\frac{\partial T}{\partial t} = \nabla \cdot k\nabla T - \rho_b c_b \omega_b (T - T_b) + Q_m + Q_p \quad (7)$$

where ρ, c, T, and k are the density (kg/m^3), specific heat capacity [J/(kg·K)], temperature (K), and thermal conductivity [W/(m·K)] of the tissue, respectively; ρ_b, c_b, T_b, and ω_b are the density (kg/m^3), specific heat capacity [J/(kg·K)], temperature (K), and blood perfusion rate (s^{-1}) of the blood, respectively; the term [$\rho_b c_b \omega_b$(T − T$_b$)] simulates the heat sink effect caused by small capillaries; Q_m represents the heat generated by metabolism (W/m^3), which is less influential compared to other applied heat source terms and is often neglected; Q_p is the heat source term during thermal ablation (W/m^3), i.e., the heat generated by laser light energy deposition.

To characterize the heat transfer properties between vessels and tissues, internal forced convective heat transfer conditions were set in COMSOL to simulate the effect of vessels on temperature distribution and coagulation zones [21], and the temperature and heat fluxes were assumed to be continuous at all interfaces. The heat transfer between vessels and tissues can be described by Newton's equation [22], as shown in Equation (8):

$$-n\cdot(-k\nabla T(x,t)) = h_b(T_b - T(x,t)) \quad (8)$$

where h_b represents the heat transfer coefficient [W/(m^2·K)]. Blood is assumed to be a non-compressible Newtonian fluid with a steady laminar flow, neglecting the effect of shear effects [23]. According to Murray's law, the relationship between the tube diameter and the flow in the lumen [24] is obtained by assuming that the vascular flow depends on the vascular radius r, as shown in (9):

$$Q = \left(\frac{1024\mu}{d_i^6 \pi^2 \xi\left[\rho_{tube}(c^2 + 2c) + \rho_{fluid}\right]}\right)^{-1/2} \quad (9)$$

where d_i is the vessel diameter (mm), μ is the dynamic viscosity of the fluid (Pa·s), ξ is the power-to-mass ratio of the pumping system, c is the constant material property of the pipe, and the constants ρ_{tube} and ρ_{fluid} are the pipe material density and fluid density, respectively. $\xi[\rho_{tube}(c^2 + 2c) + \rho_{fluid}]$ is a constant 93.44 kgs^{-3} m^{-1} [13]. Thus, the intravascular flow velocity is

$$S = Q/\left(\pi r^2\right) \quad (10)$$

The Arrhenius model is often the gold standard for thermal damage scenarios because it considers the time factor to represent the relationship between protein thermal degradation and tissue damage at the threshold temperature and time reached. The specific equation is shown in Equation (11) [25]:

$$\Omega t = \int_0^t A e^{-\frac{E_a}{RT}} dt \quad (11)$$

where $\Omega(t)$ is the degree of tissue death (or damage integral), t is the ablation time (s), A is the frequency factor (s^{-1}), E_a is the activation energy (J/mol), R is the universal gas constant (8.314 J/mol·K), and T is the tissue temperature (K) in the computational domain at the specified time.

The photothermal effect of tissue during ablation is a complex process in which the tissue's optical and thermal physical parameters undergo reversible and irreversible dynamic changes with increasing temperature and decreasing water content in the tissue, which ultimately affects the ablation [26]. The changes in the optical properties of the

tissue are mainly caused by coagulation, i.e., $\Omega(t)$ is the degree of tissue death (or damage integral), and thermal damage is defined as a logarithmic function of the concentration ratio of the original tissue molecules to the remaining undamaged tissue molecules $C(t)$, thus defining the concentration ratio between undamaged and original undamaged tissue at time t as F_u and the concentration ratio between damaged and original undamaged tissue as F_d, specifically expressions are given in Equations (12) and (13) [27,28]:

$$F_u = \frac{C(t)}{C(t_0)} = exp(-\Omega) \tag{12}$$

$$F_d = \frac{C(t_0) - C(t)}{C(t_0)} = 1 - exp(-\Omega) \tag{13}$$

The range of F_u is 1 for pristine tissue and 0 for fully damaged tissue, and the range of F_d is the opposite. The dynamic optical parameters can be determined by summing the concentration ratios of damaged and undamaged tissues, respectively, and the product of the corresponding optical properties at the two extremes, with the subscript native indicating undamaged values and the subscript denatured indicating damaged values, as expressed in Equations (14)–(16) [27,28]:

Absorption coefficient

$$\mu_a = F_u \cdot \mu_{a,native} + F_d \cdot \mu_{a,denatured} = exp(-\Omega) \cdot \mu_{a,native} + (1 - exp(-\Omega)) \cdot \mu_{a,denatured} \tag{14}$$

Scattering coefficient

$$\mu_s = F_u \cdot \mu_{s,native} + F_d \cdot \mu_{s,denatured} \tag{15}$$

Anisotropy factor

$$g = F_u \cdot g_{native} + F_d \cdot g_{denatured} \tag{16}$$

Brain tissue is rich in water content, and although accurate data on temperature-dependent and damage-dependent thermal physical parameters are lacking, the thermal properties of the tissue can be approximated based on the dynamic changes in the thermal properties of water content and water in the range of 20–100 °C [28,29], as expressed in Equations (17)–(19) [29]:

$$\rho(T) = \rho_0(1.3 - 0.3k_\rho w) \tag{17}$$

$$c(T) = c_0(0.37 + 0.63k_c w) \tag{18}$$

$$k(T) = k_0(0.133 + 1.36k_k w) \tag{19}$$

where ρ_0 is the initial value of density of brain tumor/brain tissue (kg/m^3), c_0 is the initial value of specific heat capacity [J/(kg·K)], k_0 is the initial value of thermal conductivity [W/(m·K)]; w denotes the water content of brain tissue (%), taken as 0.85; k_ρ, k_c, and k_k denote the proportionality coefficients of density, specific heat capacity, and thermal conductivity of water with temperature, respectively, and the specific expressions are shown in Equations (20)–(22) [29]:

$$k_\rho = 1 - 4.98 \times 10^{-4}(\mathrm{T} - 20\ ^\circ\mathrm{C}) \tag{20}$$

$$k_c = 1 + 1.016 \times 10^{-4}(\mathrm{T} - 20\ ^\circ\mathrm{C}) \tag{21}$$

$$k_k = 1 + 1.78 \times 10^{-3}(\mathrm{T} - 20\ ^\circ\mathrm{C}) \tag{22}$$

2.3. Boundary and Initial Conditions

In the simulation, the initial temperature of the biological tissue is 37 °C, and the initial temperature of the laser fiber is 27 °C. The laser is selected as Nd: YAG near-infrared light with a wavelength of 1064 nm, the power is dynamically adjusted with PID control, the maximum temperature is maintained at no more than 90 °C, and the ablation time is 400 s. The Dirichlet boundary conditions are set at the fiber, and biological tissue boundaries, the inlet velocity of the vessel is determined by the lumen diameter, and the outlet pressure is 0 Pa. Table 1 lists the dynamic changes of tissue properties with increasing temperature during heating and the material properties of the whole model. The properties of the fiber are listed in Table 2, and the radius parameters of the vessel are listed in Table 3.

Table 1. Optical properties and thermal physical parameters of tissues and blood vessels [30,31].

Parameter	Brain		Blood
	Native	Denatured	
Absorption coefficient, μ_a (1/m)	50	62	883
Scattering coefficient, μ_s (1/m)	6700	7890	14,201
Anisotropy factor, g	0.96	0.93	0.98
Density, ρ (kg/m^3)	1040		1050
Specific heat capacity, c (J/(kg·K))	3590		4180
Thermal conductivity, k (W/(m·K))	0.503		0.517
Dynamic viscosity, μ (Pa·s)	-		0.00365

Table 2. Characteristic parameters of optical fibers [32].

Parameter	Fiber Core	Thin Layer
Absorption coefficient, μ_a (1/m)	-	266
Scattering coefficient, μ_s (1/m)	-	3000
Anisotropy factor, g	-	0.98
Density, ρ (kg/m^3)	2203	2203
Specific heat capacity, c (J/(kg·K))	703	703
Thermal conductivity, k (W/(m·K))	1.38	1.38

Table 3. Radius parameters of blood vessels [13].

No.	Radius, r (mm)	No.	Radius, r (mm)
1	0.1	6	0.6
2	0.2	7	0.7
3	0.3	8	0.8
4	0.4	9	0.9
5	0.5	10	1.0

3. Result

During LITT thermal ablation, as the vessel diameter increases, (i) the cooling coagulation effect of the temperature field on the vessel becomes worse, and (ii) the directional effect of the temperature field influenced by the vessel diminishes.

3.1. Temperature Field Variation at Different Vessel Radii

We used Ω = 1 as the ablation zone boundary [33] and analyzed the ablation of vessels with a radius of 0.1–1.0 mm at the end (at the red line), as shown in the thermal damage location map of the vessel in Figure 5, with blood flowing from A to B and flow rate varying with the vessel diameter. Figure 6a–j shows the thermal damage of the end section of the vessel at a distance of 1 mm between the fiber and the vessel, at a maximum temperature of 90 °C and 400 s of ablation, and the green line indicates the range of loss. As can be seen

from the Figure 6, the end cross-section of the 0.1–0.3 mm radius vessel was completely coagulated; the 0.4 mm vessel had 90% coagulation, the 0.5–0.6 mm vessel continued to decrease in the coagulation range and suffered partial thermal damage, but not enough to cause blood flow blockage; and the 0.7–1.0 mm vessel blood was not affected in any way. The temperature field had a coagulation effect on the vessels; at a constant distance from the fiber, the vessel coagulation decreased with increasing radius, indicating that the vessels carried more heat from the temperature field.

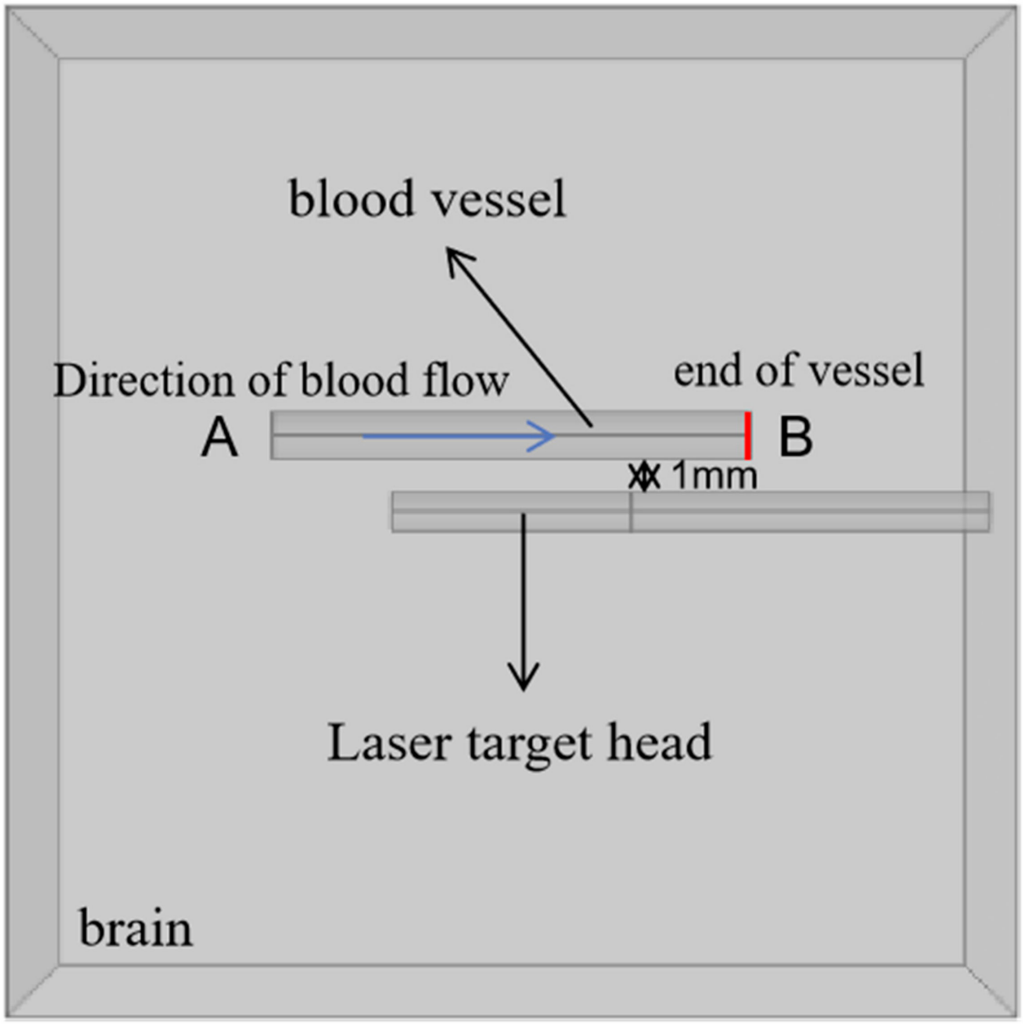


Figure 5. Location of vascular thermal injury.

When performing precise intracranial thermal ablation, the target temperature of LITT was set at 45–90 °C [5] to achieve the ablation temperature without causing vaporization due to high temperature and adhesion of residual tissue in fiber retraction. The maximum temperature was controlled by PID not to exceed 90 °C, and $\Omega = 1$ was used as the ablation boundary for 400 s. Figure 7a–j shows the effect of different vessel radii 0.1–1.0 mm on the ablation temperature field, and Figure 7k shows the actual ablation temperature plot without the influence of vessels. The Figure 7 show that small vessels' effect on the temperature field is also worthy of attention, which will produce obvious directional effects. The blood flow in the vessels of radius 0.1–0.2 mm is completely coagulated, the directional effect is not obvious, and the damaged area is ellipsoidal; the temperature field at radius 0.3–0.6 mm has obvious characteristics of moving in the direction of blood flow and forming a tail-like structure; at a radius of 0.7–1.0 mm, the directional effect of the temperature field is only spread against the vascular wall, and there is no thermal damage to the blood

vessels. At a constant distance from the fiber, the directional effect of the vessel on the temperature field decreases as the radius increases.

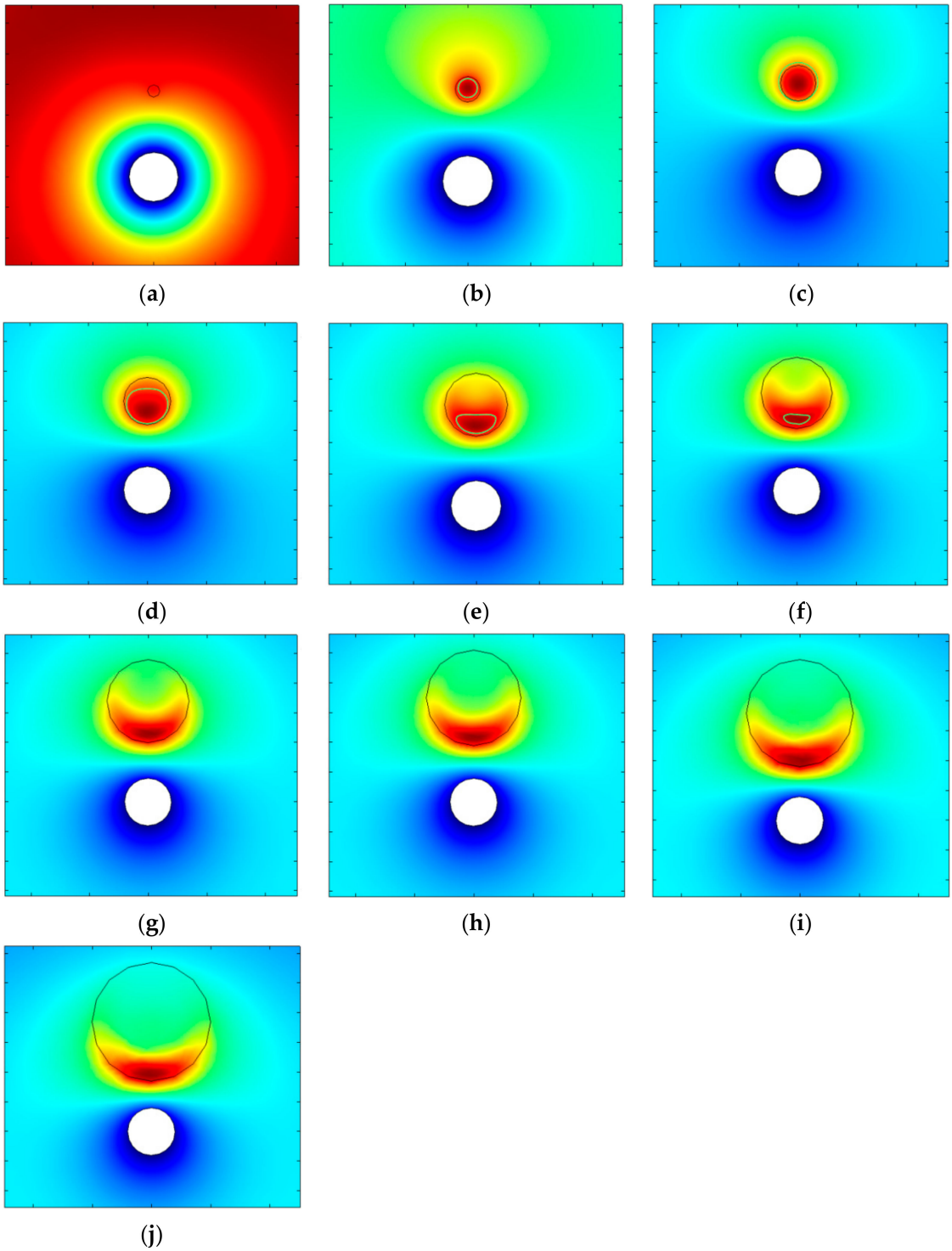


Figure 6. Thermal damage located at the end cross-section of the vessel (**a**–**j**) indicates vessels with a radius of 0.1–1.0 mm, the green line indicates the range of loss, and the color indicates the temperature (The temperature map transitions from high (red) to low (blue) by color). (**a**) r = 0.1 mm, (**b**) r = 0.2 mm, (**c**) r = 0.3 mm, (**d**) r = 0.4 mm, (**e**) r = 0.5 mm, (**f**) r = 0.6 mm, (**g**) r = 0.7 mm, (**h**) r = 0.8 mm, (**i**) r = 0.9 mm, (**j**) r = 1.0 mm.

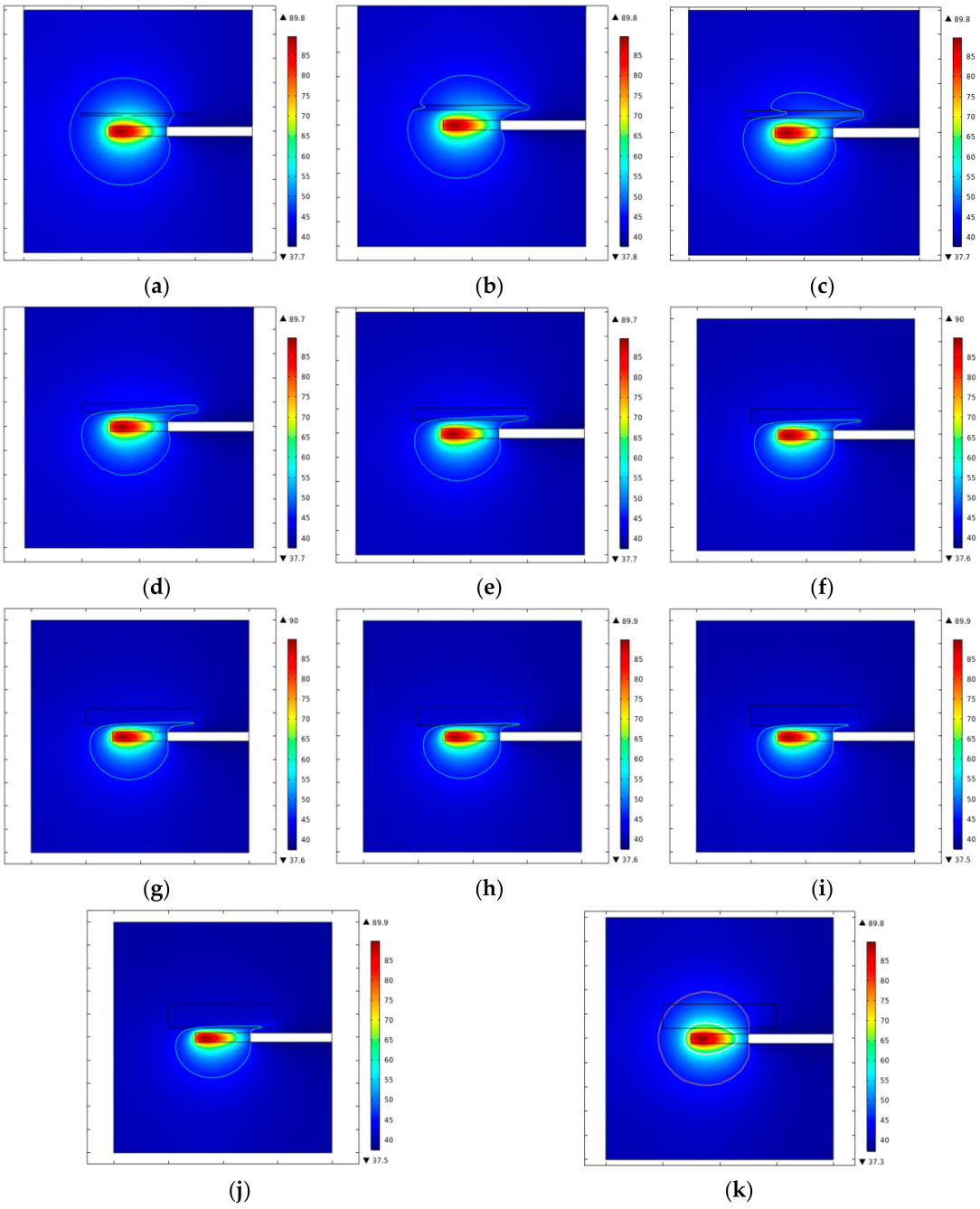


Figure 7. LITT temperature field distribution (**a**–**j**) indicates the effect of vessels with a radius of 0.1–1.0 mm on the ablation temperature field, (**k**) indicates the temperature field without the effect of vessels, and the green line indicates the loss range. (**a**) r = 0.1 mm, (**b**) r = 0.2 mm, (**c**) r = 0.3 mm, (**d**) r = 0.4 mm, (**e**) r = 0.5 mm, (**f**) r = 0.6 mm, (**g**) r = 0.7 mm, (**h**) r = 0.8 mm, (**i**) r = 0.9 mm, (**j**) r = 1.0 mm, (**k**) No vascular effects.

Based on the above, a simple classification of blood vessels can be made, as shown in Figure 8. Vessels with 0.1–0.2 mm radius range clotting leading to early blood flow obstruction, 0.3–0.6 mm vessels with cooling and directional effects on the temperature field, and 0.7–1.0 mm vessels taking away a large amount of heat affecting the distribution of the temperature field, but without the clotting effect of vessels and directional effects of the temperature field, can be modeled as similar to solid tissues, giving different material properties.

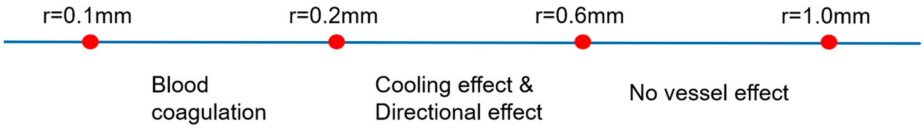


Figure 8. Classification diagram of the effect of micro-vessels on ablation effect (distance between fiber and vessel is 1 mm).

3.2. Temperature Field Variation for Different Fiber-to-Vessel Distances

The distance between the fiber and the vessel is also an important factor affecting the change in the temperature field. It is known from the study of 3.1 that the temperature field is most obviously affected by the directional effect of the vessel with a 0.3–0.6 mm radius, while the spacing of 1 mm, 2 mm, and 3 mm is chosen for the study (Figure 9). Therefore, the highest temperature is controlled by PID not to exceed 90 °C, and Ω = 1 is taken as the ablation boundary for 400 s. Figure 10 shows the temperature field distribution of the same vessel radius in temperature field distribution at different spacing with the same radius in the same row plot and the same distance in the same column plot. It can be seen from the Figure 10 that the directional of the temperature field influenced by the vessels decreases as the distance between the fiber and the vessels increases, and the directional effect is produced by the vessels of radius 0.3–0.4 mm at a distance of 2 mm; at a distance of 3 mm, only the vessels of radius 0.3 mm produce the directional effect; and the ablation zone is gradually symmetrical from left to right as the distance between the fiber and the vessels increases.

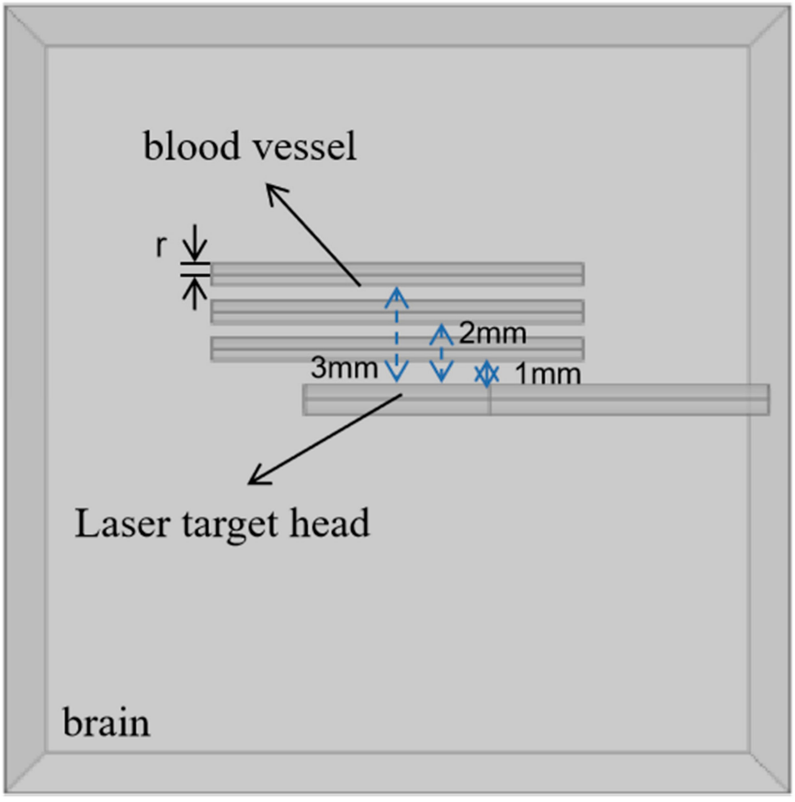


Figure 9. Model diagram of the distance between different fibers and blood vessels.

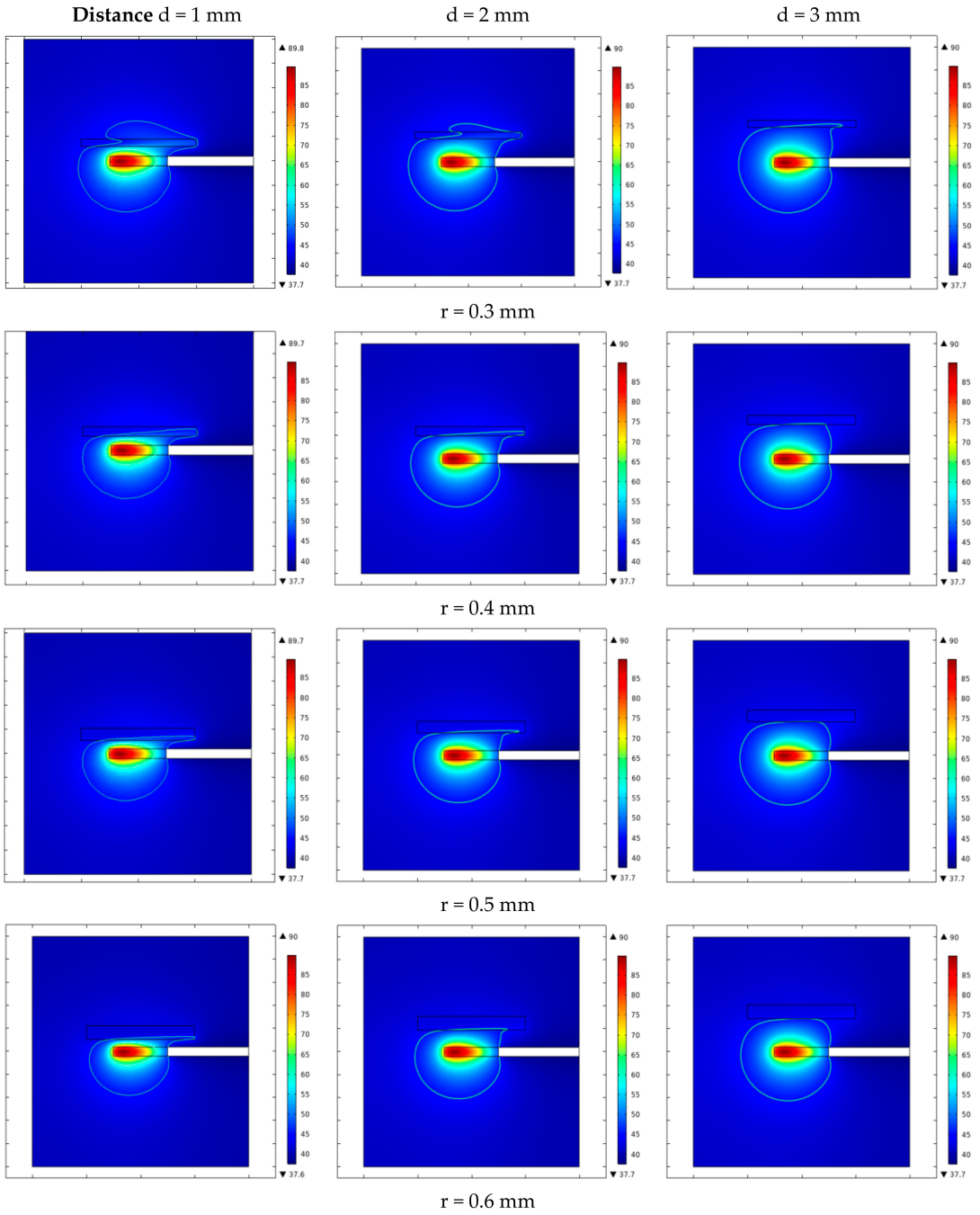


Figure 10. Temperature field distribution at different distances, each row indicates the same vessel radius of 0.3–0.6 mm, each column indicates the same distance between the fiber and the vessel of 1–3 mm, and the green line indicates the loss range.

4. Discussion

As the most delicate organ in the whole body, the brain has a complex nervous system and blood vessel system; the existing multi-physics field modeling rarely takes into account the directional effect of isolated vessels (especially tiny vessels) on the temperature field, i.e., the same directional effect as the blood flow direction, which affects the correct assessment of the temperature field and the region of thermal damage.

In this paper, we focus on the relationship between the temperature field of LITT and micro-vessels, applying the PID control equation to fix the maximum temperature at 90 °C, using dynamic photothermal parameters to make the simulation more realistic, setting the blood flow rate related to the vessel diameter, which is not a fixed value between each vessel,

the larger the diameter of the vessel the higher the flow rate, and the formula calculates that the flow rate is proportional to the radius is also greater. Thermal ablation is known to cause tiny blood vessels to coagulate, and blood vessels have cooling and directional effects on temperature fields. The results show that at a distance of 1 mm between the fiber and the vessel, the smaller the vessel radius, the more pronounced the coagulation effect. Vascular radii between 0.3 and 0.6 mm have significant cooling and directional effects. The cooling effect is the key reason why the influence of heat diffusion on temperature distribution grows as the vascular radius rises. From this, the blood vessels are classified, focusing on the vascular radius, which directly affects the temperature distribution. By further changing the vessel-fiber spacing, it is found that there is no directional effect in the combination of (r = 0.4, d = 3), (r = 0.5, d = 2), (r = 0.5, d = 3), (r = 0.6, d = 2), (r = 0.6, d = 3), indicating that the temperature field affected by blood flow decreases with the increase of vessel-fiber spacing. The ablation shape gradually tends to be symmetrical. This provides certain guidance for LITT numerical simulation. For example, when small vessels are encountered during ablation, vascular diameter and the distance between vessels and optical fibers are considered at the same time to reduce the influence of directional effect on temperature distribution, to achieve the objective of ablation without damaging blood vessels, and contribute to the accuracy of preoperative planning.

However, our preliminary study also has some limitations. The classification of blood vessels in this paper relies only on the radius parameter and does not consider more factors, and the fiber optic parameter settings are fixed. To further improve the simulation accuracy, the setting of convective heat transfer coefficients between the vessel surface and the tissue needs further investigation while adding a control with ex vivo experiments. In subsequent studies, these factors will be added to the simulations to investigate the key parameters that ultimately affect the temperature distribution.

5. Conclusions

By establishing a PID control Laser Interstitial Thermal Therapy brain tissue model with appropriate settings of dynamic photothermal parameters and changing blood flow parameters, the multi-physical field coupling of optical, flow, and temperature fields was performed to determine the interplay between vascular and temperature distribution and thermal damage: (1) coagulation effect, (2) cooling effect and directional effect. The addition of blood vessels leads to asymmetry of temperature distribution in the ablation zone and the preliminary classification of blood vessels to obtain the directional effect of temperature distribution between the approximate radius of blood vessels 0.3–0.6 mm. The larger the distance between fiber and blood vessels, the more the temperature field shape tends to be symmetrical to the left and right, providing a reference for accurate prediction of temperature change and damage. In the future, we will also consider adding tumor models to obtain a wider range of clinical treatment parameters.

Author Contributions: S.B., idea proposal, data analysis, simulation, writing-original manuscript preparation, review, and editing; Q.N., supervision, conceptualization, investigation, project administration, funding acquisition, visualization, validation, writing—review, and editing; H.L., conceptualization, review of the manuscript; X.M. conceptualization, review of the manuscript. All authors have read and agreed to the published version of the manuscript.

Funding: This work was supported by the National Natural Science Foundation of China (31771021, 11832003).

Institutional Review Board Statement: Not applicable.

Informed Consent Statement: Not applicable.

Conflicts of Interest: The authors declare no conflict of interest.

References

1. Davis, F.G.; Mccarthy, B.J. Epidemiology of brain tumors. *Curr. Opin. Neurol.* **2000**, *13*, 635–640. [CrossRef]
2. Yan, J.F.; Liu, J. Cryosurgery and hyperthermia treatment on brain tumors and the thermal issues involved. *Beijing Biomed. Eng.* **2006**, *25*, 325–329.
3. Franck, P.; Henderson, P.W.; Rothaus, K.O. Basics of lasers: History, physics, and clinical applications. *Clin. Plast. Surg.* **2016**, *43*, 505–513. [CrossRef] [PubMed]
4. Menovsky, T.; Beek, J.F.; Van Gemert, M.J.C.; Roux, F.X.; Bown, S.G. Interstitial laser thermotherapy in neurosurgery: A review. *Acta Neurochir.* **1996**, *138*, 1019–1026. [CrossRef]
5. Ye, Y.Y. *Experimental Study and Device Design of Thermal Damage by Laser Action on Biological Tissues*; South China University of Technology: Guangzhou, China, 2020.
6. Wang, X.R.; Gao, H.J.; Wu, S.C.; Bai, Y. Review of simulation techniques for radiofrequency ablation of liver tumor. *Chin. Med. Devices* **2018**, *33*, 108–114.
7. Marqa, M.F.; Mordon, S.; Betrouni, N. Laser interstitial thermotherapy of small breast fibroadenomas: Numerical simulations. *Lasers Surg. Med.* **2012**, *44*, 832–839. [CrossRef] [PubMed]
8. Nishii, T.; Kotoko, A.; Hori, Y.; Matsuzaki, Y.; Watanabe, Y.; Morita, Y.; Kono, A.K.; Matsuda, H.; Fukuda, T. Filtered back projection revisited in low-kilovolt computed tomography angiography: Sharp filter kernel enhances visualization of the artery of Adamkiewicz. *Neuroradiology* **2019**, *61*, 305–311. [CrossRef] [PubMed]
9. Sheu, T.W.H.; Solovchuk, M.A.; Chen, A.W.J.; Thiriet, M. On an acousticsthermal-fluid coupling model for the prediction of temperature elevation in liver tumor. *Int. J. Heat Mass Transf.* **2011**, *54*, 4117–4126. [CrossRef]
10. Andreozzi, A.; Brunese, L.; Iasiello, M.; Tucci, C.; Vanoli, G.P. A novel local thermal non-equilibrium model for biological tissue applied to multipleantennas configurations for thermal ablation. *Numer. Heat Transf. Part A Appl.* **2021**, *79*, 111–121. [CrossRef]
11. Hassanpour, S.; Saboonchi, A. Modeling of heat transfer in a vascular tissue-like medium during an interstitial hyperthermia process. *J. Therm. Biol.* **2016**, *62*, 150–158. [CrossRef]
12. Huang, W.H. Influence of blood vessel on the thermal lesion formation during radiofrequency ablation for liver tumors. *Med. Phys.* **2013**, *40*, 073303. [CrossRef]
13. Vaidya, N.; Baragona, M.; Lavezzo, V.; Maessen, R.; Veroy, K. Simulation study of the cooling effect of blood vessels and blood coagulation in hepatic radio frequency ablation. *Int. J. Hyperth.* **2021**, *38*, 95–104. [CrossRef] [PubMed]
14. Chen, H.B. *PID Control Temperature Feedback Photothermal Treatment System Based on Infrared Thermal Imager*; Fujian Normal University: Fuzhou, China, 2019.
15. Zhu, F.L. *Simulation and Experimental Monitoring of Temperature Field in Laser Induced Interstitial Hyperthermia*; Fujian Normal University: Fuzhou, China, 2018.
16. Kerbage, Y.; Rouillès, J.; Vignion, A.S.; Delhem, N.; Thecua, E.; Deleporte, P.; Collinet, P.; Mordon, S. Laser interstitial thermotherapy (LITT) for breast cancer: Dosimetry optimization and numerical simulation. *Lasers Med. Sci.* **2022**, *37*, 489–498. [CrossRef] [PubMed]
17. Nguyen, T.H.; Park, S.; Hlaing, K.K.; Kang, H.W. Temperature feedback-controlled photothermal treatment with diffusing applicator: Theoretical and experimental evaluations. *Biomed. Opt. Express* **2016**, *7*, 1932–1947. [CrossRef]
18. Li, L.; Dong, W.W.; Shi, P.; Gan, A.; Xu, Q. Thermal effect of high power Yb: YAG microlaser. *Laser Technol.* **2010**, *34*, 8–12.
19. Du, W.; Wang, L.T.; Wang, J.Y.; Zhang, X. Transverse intensity distribution of output beam of fiber coupled semiconductor laser based on super Gaussian function. *Henan Sci. Technol.* **2022**, *41*, 39–43.
20. Miaskowski, A.; Gas, P. Numerical Estimation of SAR and Temperature Distributions inside Differently Shaped Female Breast Tumors during Radio-Frequency Ablation. *Materials* **2022**, *16*, 223. [CrossRef] [PubMed]
21. Van Leeuwen, G.M.; Kotte, A.N.; Raaymakers, B.W.; Lagendijk, J.J. Temperature simulations in tissue with a realistic computer-generated vessel network. *Phys. Med. Biol.* **2000**, *45*, 1035–1049. [CrossRef] [PubMed]
22. Consiglieri, L.; Santos, I.D.; Haemmerich, D. Theoretical analysis of the heat convention coefficient in large vessels and the significance for thermal ablative therapies. *Phys. Med. Biol.* **2003**, *48*, 4125–4134. [CrossRef] [PubMed]
23. Sutera, S.P.; Skalak, R. The history of poiseuille's law. *Annu. Rev. Fluid Mech.* **1993**, *25*, 19. [CrossRef]
24. Williams, H.R.; Trask, R.S.; Weaver, P.M.; Bond, I.P. Minimum mass vascular networks in multifunctional materials. *J. R. Soc. Interface* **2008**, *5*, 55–65. [CrossRef]
25. Gas, P.; Kurgan, E. Evaluation of Thermal Damage of Hepatic Tissue During Thermotherapy based on the Arrhenius Model. In Proceedings of the Progress in Applied Electrical Engineering (PAEE), IEEE Conference, Koscielisko, Poland, 18–22 June 2018; pp. 1–4.
26. Rossmanna, C.; Haemmerich, D. Review of temperature dependence of thermal properties, dielectric properties, and perfusion of biological tissues at hyperthermic and ablation temperatures. *Crit. Rev. Biomed. Eng.* **2014**, *42*, 467–492. [CrossRef]
27. Martelli, F.; Sassaroli, A.; Yamada, Y.; Zaccanti, G. Analytical approximate solutions of the time-domain diffusion equation in layered slabs. *J. Opt. Soc. Am. A Opt. Image Sci. Vis.* **2002**, *19*, 71–80. [CrossRef]
28. Jiang, S.C.; Zhang, J.Z.; Zhang, X.X. Parameter selection in laser-induced tumor interstitial hyperthermia based on a dynamic photothermal model. *Acta Laser Biol. Sin.* **2006**, *15*, 221–227.
29. Kim, B.M.; Jacques, S.L.; Rastegar, S.; Thomsen, S.; Motamedi, M. Nonlinear finite-element analysis of the role of dynamic changes in blood perfusion and optical properties in laser coagulation of tissue. *IEEE J. Sel. Top. Quantum Electron.* **1997**, *2*, 922–933.

30. Amini, S.; Ahmadikia, H. New approach of controlling the area affected in brain tumour treatment by LITT. *Comput. Methods Biomech. Biomed. Eng.* **2021**, *24*, 1221–1227. [CrossRef]
31. Chen, R.; Xie, S.S.; Chen, Y.J.; Lin, A.; Li, D. Tissue optical parameters of Chinese blood. *Optoelectron. Laser* **2002**, 92–93+97.
32. Fasano, A.; Homberg, D.; Naumov, D. On a mathematical model for laser-induced thermotherapy. *Appl. Math. Model.* **2010**, *34*, 3831–3840. [CrossRef]
33. Zhang, B.; Moser, M.A.J.; Zhang, E.M.; Luo, Y.; Liu, C.; Zhang, W. A review of radiofrequency ablation: Large target tissue necrosis and mathematical modelling. *Phys. Med.* **2016**, *32*, 961–971. [CrossRef] [PubMed]

Disclaimer/Publisher's Note: The statements, opinions and data contained in all publications are solely those of the individual author(s) and contributor(s) and not of MDPI and/or the editor(s). MDPI and/or the editor(s) disclaim responsibility for any injury to people or property resulting from any ideas, methods, instructions or products referred to in the content.